Electrochimica Acta 168 (2015) 261–270

Contents lists available at ScienceDirect

Electrochimica Acta

journal homepage: www.elsevier.com/locate/electacta

Fluoroethylene Carbonate as Electrolyte Additive for Improving the electrochemical performances of High-Capacity $Li_{1.16}[Mn_{0.75}Ni_{0.25}]_{0.84}O_2$ Material

Yang Li [a], Fang Lian [a,*], Leilei Ma [a], Chunlan Liu [a], Lin Yang [a], Xiaomeng Sun [a], Kuochih Chou [a,b]

[a] School of Materials Science and Engineering, University of Science and Technology Beijing, Beijing 100083, PR China
[b] Department of Physical Chemistry, University of Science and Technology Beijing, Beijing 100083, PR China

ARTICLE INFO

Article history:
Received 26 January 2015
Received in revised form 6 April 2015
Accepted 6 April 2015
Available online 8 April 2015

Keywords:
Fluoroethylene carbonate
Electrolyte additive
Lithium-rich layered oxide cathode
Lithium-ion battery

ABSTRACT

The effects of a small amount of fluoroethylene carbonate ($C_3H_3FO_3$ or FEC) on the electrochemical performance of lithium-rich layered oxide cathode $Li_{1.16}[Mn_{0.75}Ni_{0.25}]_{0.84}O_2$ have been focused herein. When 1 vol.% or 2 vol.% FEC was introduced into the electrolyte, cycling performance and rate capability of $Li_{1.16}[Mn_{0.75}Ni_{0.25}]_{0.84}O_2$ have been improved, and the initial irreversible capacity (C_{irr}) loss has been lessened by suppressing the parasitic side reactions between cathode and electrolyte. However, excess FEC (5% in volume) will lead to the decreased lithium transference number (t_{Li+}), large concentration polarization and the reduced discharge capacity especially at high current. DFT calculations indicate that FEC enhances the anti-oxidation ability of the electrolyte system, and the preferential accumulation and reaction of FEC near cathode during charging due to the strong coordination between FEC and PF_6^- anion. The results from electrochemical impedance spectroscopy (EIS), X-ray photoelectron spectroscopy (XPS) and differential scanning calorimetry (DSC) measures indicate that a more stable SEI film has been formed on the cathode surface with FEC as additive, which leads to the suppression of the electrolyte aggressive decomposition and the enhancement of thermal stability.

1. Introduction

Lithium ion batteries have been applied as a power source for electric vehicles (EVs) and hybrid electric vehicles (HEVs). However, the energy/power density of the current lithium ion batteries is limited by cathode materials. Therefore, research interest has been stimulated for advanced cathodes with high specific capacity or operating voltage. Lithium-rich manganese-based layered material $Li_{1+x}[Ni_yMn_{1-y}]_{1-x}O_2$ is believed to be a promising next generation cathode material due to its high specific capacity (>250 mAh/g) and low cost compared to the conventional $LiCoO_2$ [1–4].

Nevertheless, unsatisfied cycle stability of $Li_{1+x}[Ni_yMn_{1-y}]_{1-x}O_2$ material is still one of the main problems limiting their application [5]. To deliver large discharge capacity, $Li_{1+x}[Ni_yMn_{1-y}]_{1-x}O_2$ is charged to high potential (above 4.4 V) initially which accompanied with irreversibly release of Li^+ and O^{2-} (net loss of Li_2O). The removal of Li_2O also results in rearrangement of the transition metal ions on the surface and gradually in the crystal lattice, which leads to instability of surface and structure of the material [6,7]. Moreover, our previous studies showed that the capacity degradation is derived from drastic increase of the interfacial and charge transfer resistance of the cathode upon cycling [8]. Its poor electrode/electrolyte interphase is primarily related to the aggressive oxidization of the commercial liquid electrolyte 1 M $LiPF_6$ in EC/DMC at high discharge voltage up to 4.8 V and under the existence of active oxygen [9,10]. In order to solve the problem, strategies have been proposed to stabilize the cathode crystal structure and the cathode/electrolyte interface. Coating the material with AlF_3, $FePO_4$ or ZnO is an approach to enhance structural stability of the cathode material and prevent direct contact between the active material and the electrolyte [11–14]. In addition, a native surface film mainly composed of Li_2CO_3 appears on the transition metal oxide cathode during electrode manufacturing/ processing. During the initial charging, chemical reactions occur on the interface between cathode and

* Corresponding author. Tel.: +86 10 82377985; fax: +86 10 82377985.
E-mail address: lianfang@mater.ustb.edu.cn (F. Lian).

http://dx.doi.org/10.1016/j.electacta.2015.04.030
0013-4686/

electrolyte to form SEI film consisting of the oxidation products of the electrolyte and chemical species in the native film [15]. Therefore, the stabilization of electrode/electrolyte interface by in situ forming the stabilized SEI film is also an effective route to improve the cycling performance of lithium-rich cathode $Li_{1+x}[Ni_yMn_{1-y}]_{1-x}O_2$.

Electrolyte additives for stabilizing SEI film are widely accepted as the most effective and economic route to reduce the interactions between active material and electrolyte [16]. Xiang et al. [17] reported that 1% trimethyl phosphite (TMP) enhanced capacity retention and rate capability of lithium-rich cathode $Li_{1.2}Mn_{0.54}Ni_{0.13}Co_{0.13}O_2$, since the catalyzing effect of some dissolved transition metal ions on the surface was effectively deactivated by forming the passivating interphase. Kang et al. [18] proposed 1,3,5-trihydroxybenzene (THB) as an additive to form a protective film on the cathode, and graphite/$Li_{1.10}Mn_{0.43}Ni_{0.23}Co_{0.23}O_2$ full cells could obtain a very high coulombic efficiency of greater than 99.5% after 200 cycles at 60 °C. Another additive Tris(trimethylsilyl) phosphate (TMSP) [19] can decompose at the potential 4.1 V vs. Li/Li^+, lower than that of electrolyte solvent, resulting in an artificial SEI layer tightly covered on cathode particle, leading to the improved electrochemical performances of $Li_{1.2}Ni_{0.13}Mn_{0.54}Co_{0.13}O_2$. Yang et al. [20] have used tris(hexafluoro-iso-propyl) phosphate (HFiP) as a cathode SEI former to improve the cycle and rate performances of $Li_{1.2}Mn_{0.56}Ni_{0.16}Co_{0.08}O_2$. Interestingly, LiODFB and LiBOB, which have been intensively investigated as SEI film-formation additives for anode, also showed positive impact on lithium-rich layered oxide cathodes. LiODFB electrochemically oxidized at 4.35 V vs. Li/Li^+ [21] to form passivation layers mainly containing polymerization products, which inhibited further decomposition of the electrolyte and reduced metal ions dissolution from cathode, thus depressed cell capacity loss and impedance rise [22]. Choi et al. [23] confirmed that the LiBOB-derived SEI film effectively prevented the undesirable decomposition of the electrolyte on the surface of $Li_{1.17}Ni_{0.17}Mn_{0.5}Co_{0.17}O_2$ cathodes in half and full cells with graphite anodes.

As an potential candidate of difunctional electrolyte additive for anode and cathode, fluoroethylene carbonate (FEC) has recently attracted excessive attentions due to its effective film-forming ability in improving cycle performance of the graphite and Si anodes [24–27]. Furthermore, FEC was used as SEI film-formation additive to improve the low-temperature cycle performance of cathode $LiFePO_4$ [28,29]. FEC exhibited a positive effect on cycling stability of cathode $LiCoO_2$ when charged to 4.5 V vs. Li/Li^+, which was related to the SEI film with abundant polycarbonate components formed on the cathode surface [30]. Although FEC was employed as anti-oxidative co-solvent to improve the stability of the electrolyte in 5 V cathode system [31,32], the effect of FEC on the performance of Li-rich cathode $Li_{1+x}[Ni_yMn_{1-y}]_{1-x}O_2$ has still been significantly less reported to our knowledge.

In order to optimize the electrode/electrolyte interfacial behavior, FEC as an electrolyte additive was introduced in lithium-rich cathode $Li_{1.16}[Mn_{0.75}Ni_{0.25}]_{0.84}O_2$ system, and the effect of FEC on its performance was investigated using the basic electrolyte 1 mol/L $LiPF_6$ dissolved in the mixture of ethylene

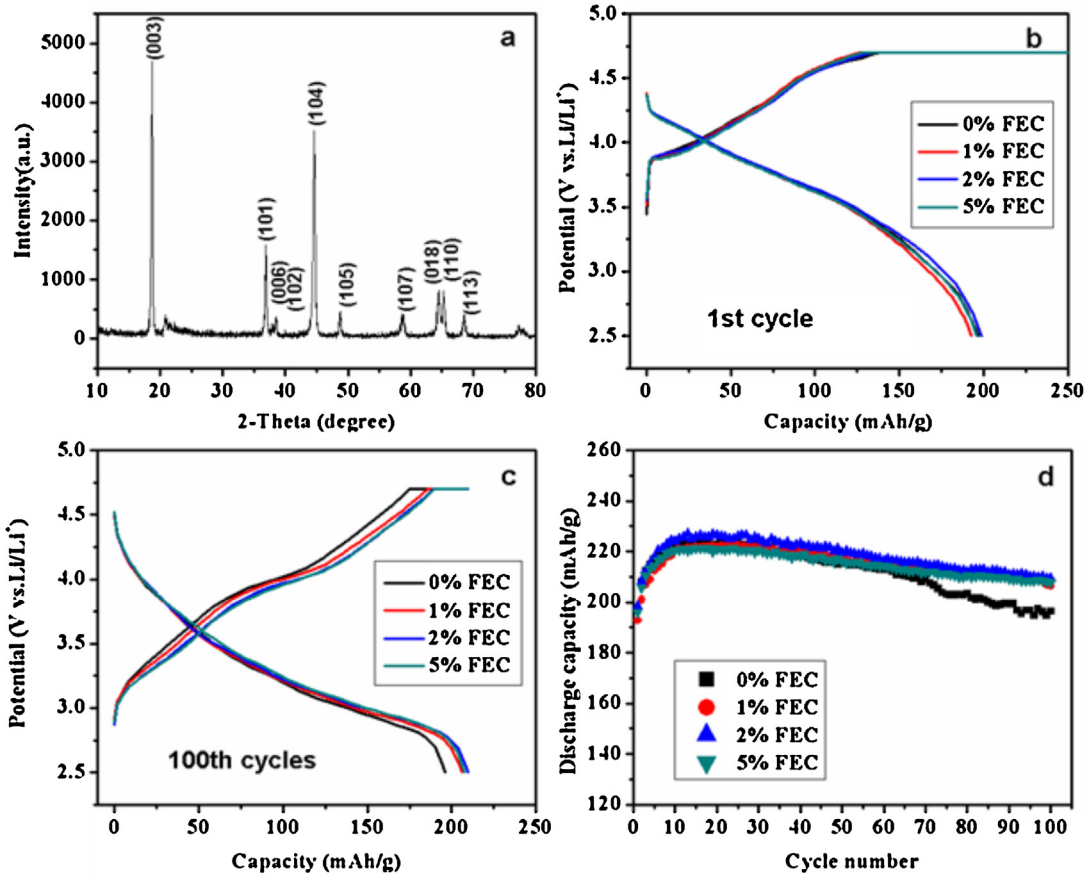

Fig. 1. XRD pattern of as-synthesized $Li_{1.16}[Mn_{0.75}Ni_{0.25}]_{0.84}O_2$ sample (a) and charge/discharge profiles of the 1st (b), 100th (c) cycle and cycling performance (d) of Li/$Li_{1.16}[Mn_{0.75}Ni_{0.25}]_{0.84}O_2$ cells at 25 °C, 2.5-4.7 V, 0.5C.

Table 1
The initial cycle data of Li/ $Li_{1.16}[Mn_{0.75}Ni_{0.25}]_{0.84}O_2$ cells in the electrolytes with various contents of FEC: at 25 °C, 2.5-4.7 V, 0.5C.

Amount of FEC (v%)	First charge capacity(mAh/g)	First discharge capacity(mAh/g)	C_{irr} (mAh/g)	Coulombic efficiency (%)
0	293.6	196.8	96.8	67.0
1	275.5	192.8	82.7	70.0
2	284.3	198.7	85.6	70.0
5	278.5	195.8	82.7	70.3

carbonate (EC)/ dimethyl carbonate(DMC)/ diethyl carbonate (DEC).

2. Experimental

The blank electrolyte is 1 M $LiPF_6$ in 1:1:1 (vol. %) EC/ DMC/ DEC solution. The electrolyte with various FEC contents (1%, 2% and 5% in volume) in the above blank solution were prepared in a dry argon filled glove box(MBraun, LABmaster glove box workstation) with mass fractions of water and oxygen below 0.5 ppm. Fluoroethylene carbonate (FEC, Adamas, >99% pure) was purchased and used without any further purification. The lithium transference number (t_{Li+}) data were estimated by chronoamperometry method using Li/Li symmetric cells on electrochemical work station (VersaSTAT3, Princeton Applied Research). The impedances were measured in the frequency range of 0.01Hz-10000 Hz, and the potentiostatic polarization experiments were done with an applied voltage of 5 mV for 1000 s.

Powder X-ray diffraction (XRD, Rigaku D/max) using Cu K radiation was used to identify the as-prepared $Li_{1.16}[Mn_{0.75}Ni_{0.25}]_{0.84}O_2$ sample. Coin cells (2032) were fabricated to characterize the electrochemical performance of the electrolyte. The cathode was prepared from 85 wt.% active material, 5 wt.% polyvinylidene difluoride (PVDF) and 10 wt.% carbon black dissolved in N-methyl-2-pyrrolidone. The slurry was coated on Al foil, and then heated at 120 °C in vacuum for 24 h. The cells were cycled between 2.5 V and 4.7 V at a constant current density of 100 mA/g (0.5C) using battery test system (Land CT 2001) at 25 °C. The cells for rate performances tests were cycled between 2.5 V and 4.7 V at 0.5C for 10 cycles to avoid the influences of capacity increase on the evaluation of rate capability. And then rate tests were carried out between 2.5 V and 4.7 V at 25 °C: charged and discharged at 0.2C for the first and last 5 cycles, charged at 0.5C and subsequently discharged at various rate (0.2C, 0.5C, 1C, 2C, 3C and 5C) respectively for other cycles.

Linear sweep voltammetry (LSV) and electrochemical impedance spectroscopy (EIS) were carried out on the electrochemical work station (VersaSTAT3, Princeton Applied Research). LSV was conducted from open circle voltage OCV to 6 V (vs. Li/Li^+) at the rate of 2 mV/s at 25 °C and equipped with three-electrode cells (working electrode: stainless steel (Φ = 1.6 mm), counter electrode: stainless steel, and reference electrode: Li). EIS of the cells was investigated at charged state of 4.0 V at the 3rd, 15th, 30th, 50th, and 100th cycles at frequency ranging from 100 kHz to 0.01 Hz under amplitude of 5 mV, and the obtained impedance spectra were fitted by Zview program.

The surface chemical components of the cycled $Li_{1.16}[Mn_{0.75}Ni_{0.25}]_{0.84}O_2$ electrodes were analyzed by X-ray photoelectron spectroscopy (XPS, Kratos AXIS Ultra DLD) with Al Kα line as an X-ray source. The discharged electrodes were detached from the cells and then washed by dimethyl carbonate (DMC) solvent to remove the residual electrolyte, finally dried under vacuum.

For differential scanning calorimetry (DSC, TA Q2000) tests, all the cells were cycled for 100th at a rate of 0.5C, followed by fully charged to 4.7 V at 0.2C. After disassembling the cells, the cathode was gently scraped from Al current collector (nearly 5 mg each), and then sealed in Al pans. All the procedure was operated in the glove box to prevent the substance oxidizing. The measurements were carried out at a heating rate of 5 °C/min.

The quantum chemistry calculations were performed on Dmol^3 package in Material Studio software. The geometry optimizations were carried out with GGA/BLYP method with DNP basis set. The frequency calculations were performed to confirm that each optimized geometry corresponded to a stationary one. The solvent effect was considered by using conductor-like screening model (COSMO). The dielectric constant of methanol (dielectric

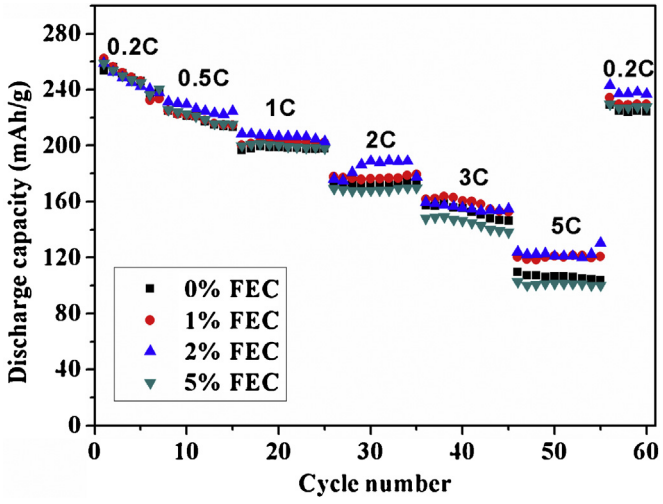

Fig. 2. Rate capability of Li/ $Li_{1.16}[Mn_{0.75}Ni_{0.25}]_{0.84}O_2$ cells in the electrolytes with various contents of FEC: at 25 °C, 2.5-4.7 V, charge and discharge at 0.2C for the first and last 5 cycles, charge at 0.5C and discharge at 0.5C-5C respectively for other cycles.

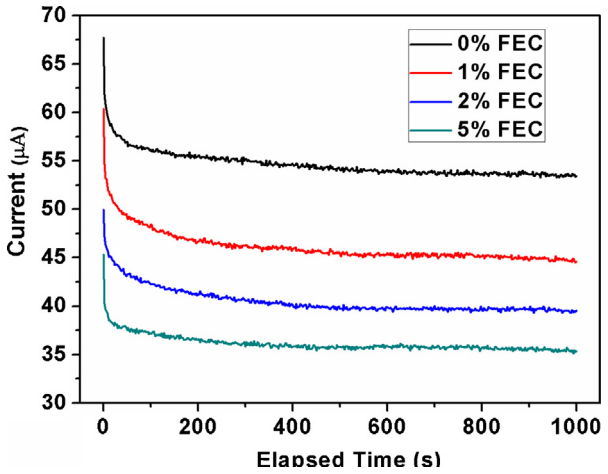

Fig. 3. DC polarization current responses of the Li/Li symmetric cells with different electrolytes.

Table 2
The measured parameters in Eq. (1) and as-calculated lithium transference numbers.

ID	I(∞)/μA	I(0)/μA	$R_{bulk}(0)/\Omega$	$R_{lithium}(0)/\Omega$	$R_{bulk}(\infty)/\Omega$	$R_{lithium}(\infty)/\Omega$	ΔV/mV	t_{Li+}
0%FEC	53.287	67.745	5.332	54.048	4.471	59.559	5	0.483
1%FEC	44.858	60.396	3.270	62.190	3.781	57.949	5	0.445
2%FEC	39.448	49.962	2.357	85.723	2.407	92.413	5	0.427
5%FEC	33.584	45.361	2.937	90.153	2.862	98.038	5	0.385

constant = 32.63) was utilized for the mixture of EC, DMC and DEC in volume ratio of 1:1:1 in the work.

3. Results and discussion

3.1. Cycle performance

Fig. 1 displays the XRD pattern of as-synthesized $Li_{1.16}[Mn_{0.75}Ni_{0.25}]_{0.84}O_2$ sample and the charge/discharge profiles of Li/$Li_{1.16}[Mn_{0.75}Ni_{0.25}]_{0.84}O_2$ cells with and without FEC additive. $Li_{1.16}[Mn_{0.75}Ni_{0.25}]_{0.84}O_2$ was prepared through a co-precipitation process [8]. All of the peaks in the XRD pattern (Fig. 1a) can be indexed based on a hexagonal α-$NaFeO_2$ structure (space group:R-3m, No.166), except for a weak reflection peak between 20° and 25° [2]. This peak is corresponded to the superlattice ordering of Li, Ni and Mn atoms in the transition metal layers for the Li-rich layered solid solution materials. The clear splitting of (0 0 6), (1 0 2) and (0 1 8), (1 1 0) peaks indicates high degree of crystallization for the as-synthesized $Li_{1.16}[Mn_{0.75}Ni_{0.25}]_{0.84}O_2$.

The charge-discharge profiles with and without FEC shown in Fig. 1b and c, appear to be similar, revealing that the lithium intercalation/de-intercalation mechanism is not altered by the FEC additive. The initial charging profiles could be divided into two stages: a smooth voltage slope in the range OCV-4.5 V, which is associated to the oxidation of Ni^{2+} to Ni^{4+}; and the voltage plateau above 4.5 V which is related to the activation of Li_2MnO_3 component along with the removal of Li_2O. During the discharge process, the reduction of Ni^{4+} to Ni^{2+} occurs before 3.5 V, and the reaction in the low voltage region (< 3.5 V) can be attributed to the reduction of Mn^{4+} ions [33,34]. After 100 cycles at 0.5C, the discharge capacity of the cells with 0%, 1%, 2% and 5% FEC are 196.4 mAh/g, 206.3 mAh/g, 209.5 mAh/g and 207.7 mAh/g, corresponding to capacity retention of 88%, 92.68%, 92.53% and 93.85% (versus the maximum discharge capacity), respectively. FEC as electrolyte additive improves the capacity retention of $Li_{1.16}[Mn_{0.75}Ni_{0.25}]_{0.84}O_2$ cells obviously and causes decrease of the cell polarization. The capacity and coulombic efficiency of the initial cycle at the current rate of 0.5C have been listed in Table 1. It can be seen that the irreversible capacity (C_{irr}) of the initial cycle reduces in the cells with FEC additive. As shown in Fig. 1d, $Li_{1.16}[Mn_{0.75}Ni_{0.25}]_{0.84}O_2$ shows the increasing discharge capacity in the early cycles. The discharge capacity increase is concentrated in the 3.5–3.0 V range. The discharge capacities delivered between 3.5 V and 3.0 V increase from 50.1 mAh/g, 48.3 mAh/g, 50 mAh/g and 53.4 mAh/g of the 1st cycle to 80.1 mAh/g, 78.3 mAh/g, 85.1 mAh/g and 78.4 mAh/g of the 10th cycle for the cathode cycled with 0%, 1%, 2% and 5% FEC, respectively. This phenomenon is attributed to the increasing available sites for the lithium insertion to the MnO_2 host structure due to the gradual activation of Li_2MnO_3 component, which was discussed deeply in our previous report [33].

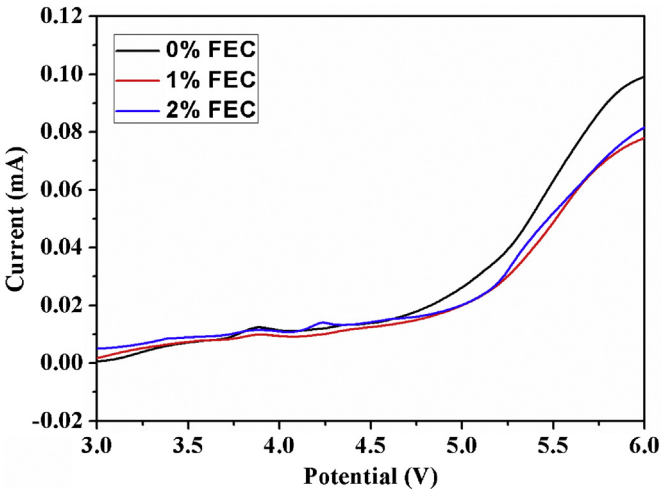

Fig. 4. The oxidation potential measurements using linear sweep voltammetry (LSV) of the electrolytes with and without FEC: at 25 °C, at the rate of 5 mV/s [Li//electrolyte//stainless steel].

3.2. Rate capability

Poor rate capability, one of the main drawbacks of lithium-rich cathode, is usually attributed to the excessive oxidation of the electrolyte at high voltage and the complicated side reaction on the cathode surface. Fig. 2 shows the rate capability of $Li_{1.16}[Mn_{0.75}Ni_{0.25}]_{0.84}O_2$ cells with and without FEC additive. $Li_{1.16}[Mn_{0.75}Ni_{0.25}]_{0.84}O_2$ cells with 1% and 2% FEC deliver high capacity of ~200 mAh/g even at 1C, while the discharge capacities of 121.6 mAh/g and 124.1 mAh/g are also achieved at 5C rate, respectively. However, cell with 5% FEC deliver only 102.8 mAh/g at 5C rate, which is lower than 109.7 mAh/g of the system without FEC. The result implies that the rate capability of the electrode $Li_{1.16}[Mn_{0.75}Ni_{0.25}]_{0.84}O_2$ can be improved with 1% and 2% FEC additive, while the increased amount (5%) of FEC reduces the discharge capacity of the cathode especially at high current density. Besides, the discharge capacities of the cells can be restored well as the low current density of 0.2C was used again.

3.3. Lithium transference number measurement (t_{Li+})

The lithium transference number (t_{Li+}) was estimated by chronoamperometry method using Li/Li symmetric cells. Applying a small constant potential to a solution by non-blocking electrodes leads to a decrease of the initial current value until a steady-state value is reached. The contribution of electrode surfaces or resistive layers variation over time can be taken into account by impedance measurements shortly before and after potentiostatic polarization [34,35]. Therefore, the lithium transference number, t_{Li+}, is calculated by Eq. (1):

Table 3
Frontier molecular orbital energy of the neutral solvent molecules and the thermodynamic properties for the solvent oxidation in gas phase.

Solvent	FEC	EC	DMC	DEC
***E*(S, HOMO)/eV**	−7.43	−6.90	−6.59	−6.41
Δ*H*/kJ/mol	1030.27	979.27	942.32	879.45
Δ*G*/kJ/mol	1026.36	976.65	940.49	874.88
ΔE_{AIE}/eV	10.77	10.27	9.92	9.31

$$S_{gas} - e^-_{gas} \xrightarrow{\Delta G(gas)} S^+_{gas}$$
$$\Delta G(solv,S) \downarrow \qquad \downarrow \qquad \downarrow \Delta G(solv,S^+)$$
$$S_{solv} - e^-_{gas} \xrightarrow{\Delta G(solv)} S^+_{solv}$$

Scheme 1. Thermodynamic cycle for the oxidation of solvated molecules.

Table 4
Calculated oxidation potentials of FEC, EC, DMC, and DEC.

	FEC	EC	DMC	DEC
in gas	9.28	8.77	8.38	7.80
ε = 32.63	6.94	6.35	6.24	5.97

Table 5
Binding energy of the formation of the ion-solvent complex.

Vacuum	FEC + PF_6^-	EC + PF_6^-	DMC + PF_6^-	DEC + PF_6^-
E_B (eV)	−0.71	−0.63	−0.25	−0.22
E_B + ΔZPE(eV)	−0.69	−0.60	−0.23	−0.21

$$t_{Li^+} = \frac{I(\infty)R_{bulk}(\infty)[\Delta V - I(0)R_{lithium}(0)]}{I(0)R_{bulk}(0)[\Delta V - I(\infty)R_{lithium}(\infty)]} \quad (1)$$

Where ΔV is the applied polarization voltage (5 mV in this study), I is the current, R_{bulk} and $R_{lithium}$ represent the respective resistances of electrolyte and the electrolyte/Li metal electrode interface, and 0 and ∞ refer to the respective initial and steady states.

Table 2 has summarized the measurement results and the calculated t_{Li+} of electrolytes. The dc polarization current responses of the Li/Li symmetric cells with different electrolytes have been displaced in Fig. 3. The values of t_{Li+} are 0.483, 0.445, 0.427 and 0.385 for electrolytes with 0%, 1%, 2% and 5% FEC, respectively. t_{Li+} values of the electrolytes decrease with the increase of FEC content in the electrolyte, which is attributed to the high viscosity of FEC (FEC: 2.3cP at 40 °C vs. EC: 1.86cP at 40 °C[36]). The cells containing 5% FEC show lower lithium transference number (t_{Li+}) and larger polarization especially at high current rate. So it is reasonable to show poorer rate capability in Fig. 2. However, the rate capability of the cells with 1% or 2% FEC addition has been improved, especially at high current density, which may be contributed to conductive interfacial film induced by FEC additive.

3.4. Oxidative stability

The oxidative decomposition behavior of FEC has been evaluated by linear sweep voltammetry (LSV). As shown in Fig. 4, no distinct oxidation peaks are observed up to about 5.1 V (versus Li/Li^+) for the electrolytes containing FEC, while the electrolyte system without FEC appears onset of current peaks near 4.8 V (versus Li/Li^+). The oxidative potentials increase 0.3 V for the electrolytes with FEC in contrast to the one without FEC. It implies a good oxidative stability of the electrolytes with FEC which are suitable for the operating voltage range for $Li_{1.16}[Mn_{0.75}Ni_{0.25}]_{0.84}O_2$ cathode.

3.5. DFT calculations

To further study the oxidative stability, the oxidation potential of EC, DMC, DEC, and FEC vs. Li/Li^+ have been calculated by the first principles method. Table 3 lists the frontier molecular orbital energy of the neutral solvent molecules and the thermodynamic properties for the solvent oxidation in gas phase. According to Frontier molecular orbital theory, the energy level of highest occupied molecular orbital (HOMO) determines the ability to lose electron, so the solvent molecules with lower HOMO energy always have higher oxidation voltage. The HOMO values of EC, DMC, DEC, and FEC in Table 3 indicate that the oxidative stability is in the order FEC>EC>DMC>DEC, which is further confirmed by the thermodynamic data of ΔH and ΔG. The adiabatic ionization energy can be defined as the energy discrepancy between the

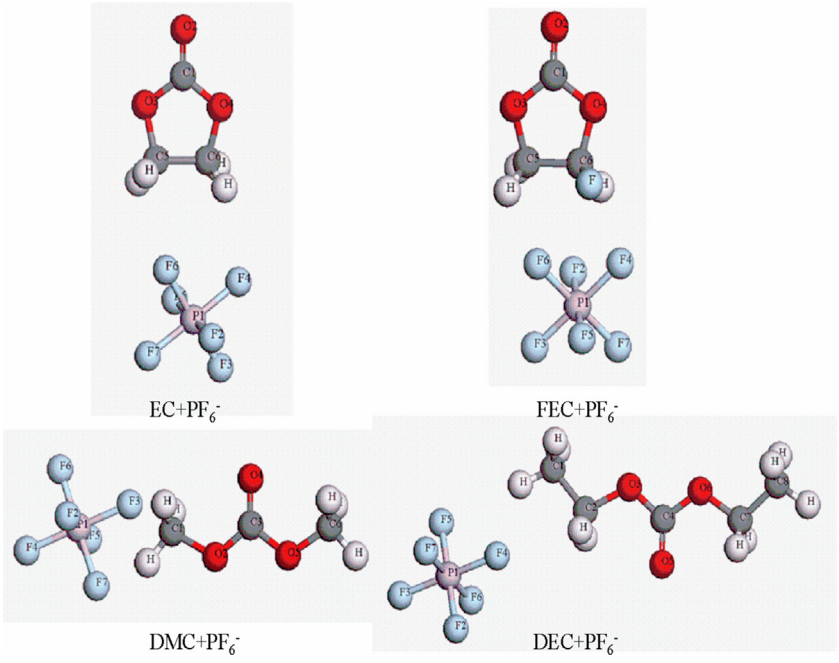

Fig. 5. Optimized geometry of the complexes of EC, FEC, DMC and DEC with PF_6^-.

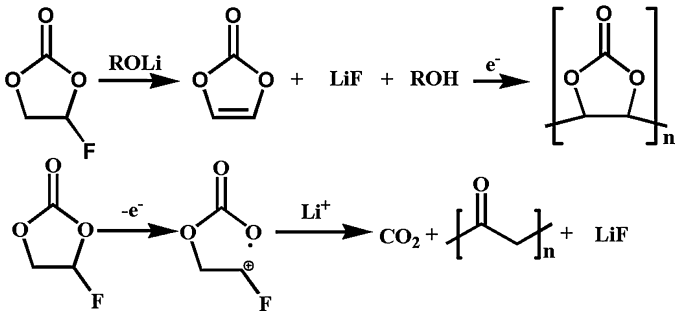

Scheme 2. Decomposition path for FEC.

optimized cation geometry and the neutral geometry: $\Delta E_{AIE} = E_c - E_n$. FEC shows the largest calculated ΔE_{AIE} in these four solvents, illustrating the highest stability of FEC against oxidation.

The Gibbs free energy changes ΔG(solv) for the oxidation of solvated molecules were determined using the thermodynamic cycle [37,38] as shown in Scheme 1. In this cycle [39,40], ΔG(solv, S) and ΔG(solv, S^+) are the solvation free energies of molecule S and its cation S^+, respectively, and ΔG(gas) is the redox energy in the gas phase. Based on these parameters, ΔG(solv) for the oxidation reaction was calculated, as shown in Eq. (2). The oxidation potential for the solvents (vs. Li/Li^+) were calculated via Eq. (3), in which the value obtained under the absolute electrochemical scale (in vacuum) minus 1.46 V to approach the experimentally measured potential vs. Li/Li^+ [39]. Table 4 has listed the calculated

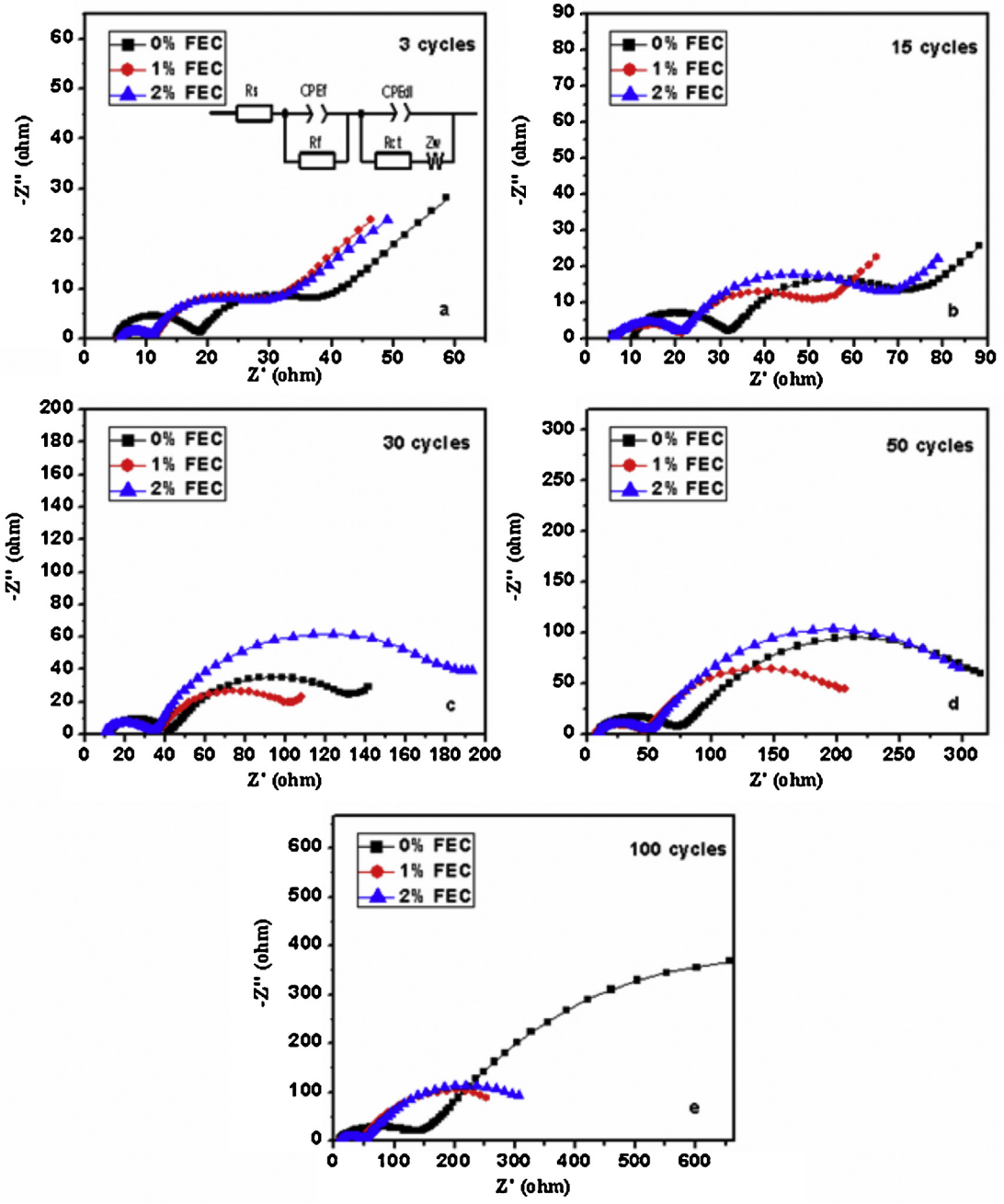

Fig. 6. EIS spectra of 50% DOC $Li_{1.16}[Mn_{0.75}Ni_{0.25}]_{0.84}O_2$ cells without FEC and with 1% and 2% FEC at 25 °C after 3 cycles(a), 15 cycles(b), 30 cycles(c), 50 cycles(d) and 100cycles (e). The inset figure describes the equivalent circuit model.

oxidation potentials of FEC, EC, DMC, and DEC. The results imply that oxidation potential of FEC is higher than the other solvents in the system, leading to an enhanced anti-oxidation ability of the electrolyte. The calculation data are consistent with the former experimental result of LSV.

$$\Delta G(solv) = \Delta G(solv,S^{+}) + \Delta G(gas) - \Delta G(solv, S) \quad (2)$$

$$E_{ox}(Li/Li^{+}) = -\Delta G(solv)/F - 1.46\,V \quad (3)$$

According to the above results, it seems that FEC is more stable against oxidation than the other solvent molecules. However, the electrolyte salt anion PF_6^- is coordinated more easily with the solvent molecules having higher dielectric constant. The interaction strength between the solvent molecule and PF_6^- anion can be quantified by calculating the binding energy of the formation of the ion-solvent complex. The optimized geometry of the complexes of EC, FEC, DMC and DEC with PF_6^- is shown in Fig. 5. The binding energy values of the complexes of FEC, EC, DMC, and DEC with PF_6^- anion in gas phase are list in Table 5. It can be found that the binding energy is in the order of FEC>EC>DEC>DMC. When the battery is charged, the negative charge in the electrolyte tends to accumulate in the vicinity of cathode. Therefore, FEC-PF_6^- reaches more easily near cathode than other solvent molecules, resulting in the preferential reaction of FEC on the cathode during charging.

3.6. Electrochemical impedance spectroscopy (EIS)

EIS measurements of $Li/Li_{1.16}[Mn_{0.75}Ni_{0.25}]_{0.84}O_2$ cells were carried out to further understand the effect of FEC on the electrode/electrolyte interfacial behavior. Fig. 6 shows the Nyquist plots of the samples with 0%, 1% and 2% FEC after different cycles. The half cells underwent specific cycles between 2.5-4.7 V at 1C rate and then charged to 4.0 V at 0.2C rate. The EIS spectra are analyzed with the equivalent circuit [8] in Fig. 6(a), which fits for the lithium intercalation/de-intercalation process in the cathode material. There are two semicircles in the diagram: the high-frequency semicircle (Rf) is attributed to Li^+ migration through the solid electrolyte interphase (SEI) film on the cathode surface, while the semicircle in medium-frequency region could be related to the charge-transfer process through the electrode/electrolyte interface (Rct). As shown in Fig. 7, the presence of FEC in the cells can dramatically suppress the growth of Rf during cycling, which implies lower migration resistance of Li-ion through SEI film. Moreover, Rf of the cell without FEC shows a much faster increase than that of the ones with 1% and 2% FEC. Rf of cells containing 1% and 2% FEC are almost unchanged after 50 cycles, indicating that the SEI films formed in the electrolyte with FEC are more stable and effectively suppress the continuous decomposition of electrolyte on the cathode surface. The cells without FEC as additive show an obvious increase of Rct upon cycling, while the ones with FEC exhibit a negligible increase of Rct. SEI layer derived from FEC protects the surface of active material from degradation. The results confirm that the presence of FEC in the cells can dramatically suppress the growth of Rf and also Rct during cycling.

3.7. X-ray photoelectron spectroscopy (XPS)

XPS spectra of C1s, F1s and P2p are displayed in Fig. 8 to study the surface composition of the cycled $Li_{1.16}[Mn_{0.75}Ni_{0.25}]_{0.84}O_2$ cathode in electrolytes with and without FEC. The C1s spectra exhibit slight differences between the cycled cathode in the electrolytes with and without FEC. The peak at 284.8 eV can be assigned to absorbed carbon from the atmosphere, peak at ~285 eV related to C–H. The peak at 286.2 eV is related to C-O, and the broad peak at 288.8 eV is related to C-O and Li_2CO_3 [41–43]. The inorganic decomposition product Li_2CO_3, a by-product of electrochemical reaction, suffering from continuous reversible change accompanied with Li^+ intercalation/deintercalation in lithium-rich manganese-based layered material [44,45], is not obvious in the C1s spectrum of cathode cycled in electrolyte with FEC. The results indicate that the formed SEI film is stabilized in the electrolyte with FEC.

The F1s spectra contain three peaks: peak at 688 eV ascribed to PVDF [28], peak at ~685 eV related to LiF [28], and peak at ~687 eV assigned to the residual $Li_xPF_y/LiPF_6$ on the surface layer [29]. Li_xPF_y is the decomposition product of $LiPF_6$ just as Eq. (4) ~ (6) [46,47]. While, LiF is normally one of the major constituents of SEI-matrix on the surface of cathode [42]. Fig. 8 shows that intensity of $Li_xPF_y/LiPF_6$ and LiF is enhanced as FEC is added. During cycling of the cells, LiF is formed due to the decomposition of FEC and $LiPF_6$ as Scheme 2 [15,48–50] and Eq. (4) ~ (10) [29,47,51]. The results suggest that a proper content of LiF was accessible to the reduced interfacial resistance and improved interfacial behavior [46,52], which is in agreement with the rate performance and EIS data of the study.

In the P2p spectra, the intensity of peak at 136.7 eV assigned to $Li_xPF_y/LiPF_6$ increases with FEC addition, which is in accordance with the F1s results. The peak at 134-135 eV related to $Li_xPF_yO_z$ is yielded from the Eq. (9) ~ (10). The decrease concentration of $Li_xPF_yO_z$ implies that the side decomposition of $LiPF_6$ has been suppressed with FEC additive in the electrolyte. The results indicate that FEC participates in the formation of a protective SEI layer, which stabilizes the electrode/electrolyte interface.

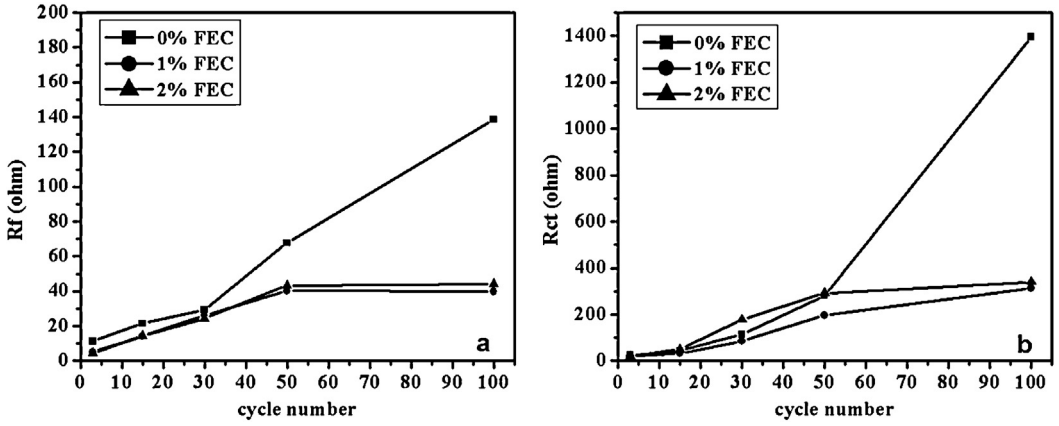

Fig. 7. The fitting results of R_f(a) and R_{ct}(b) from EIS spectra.

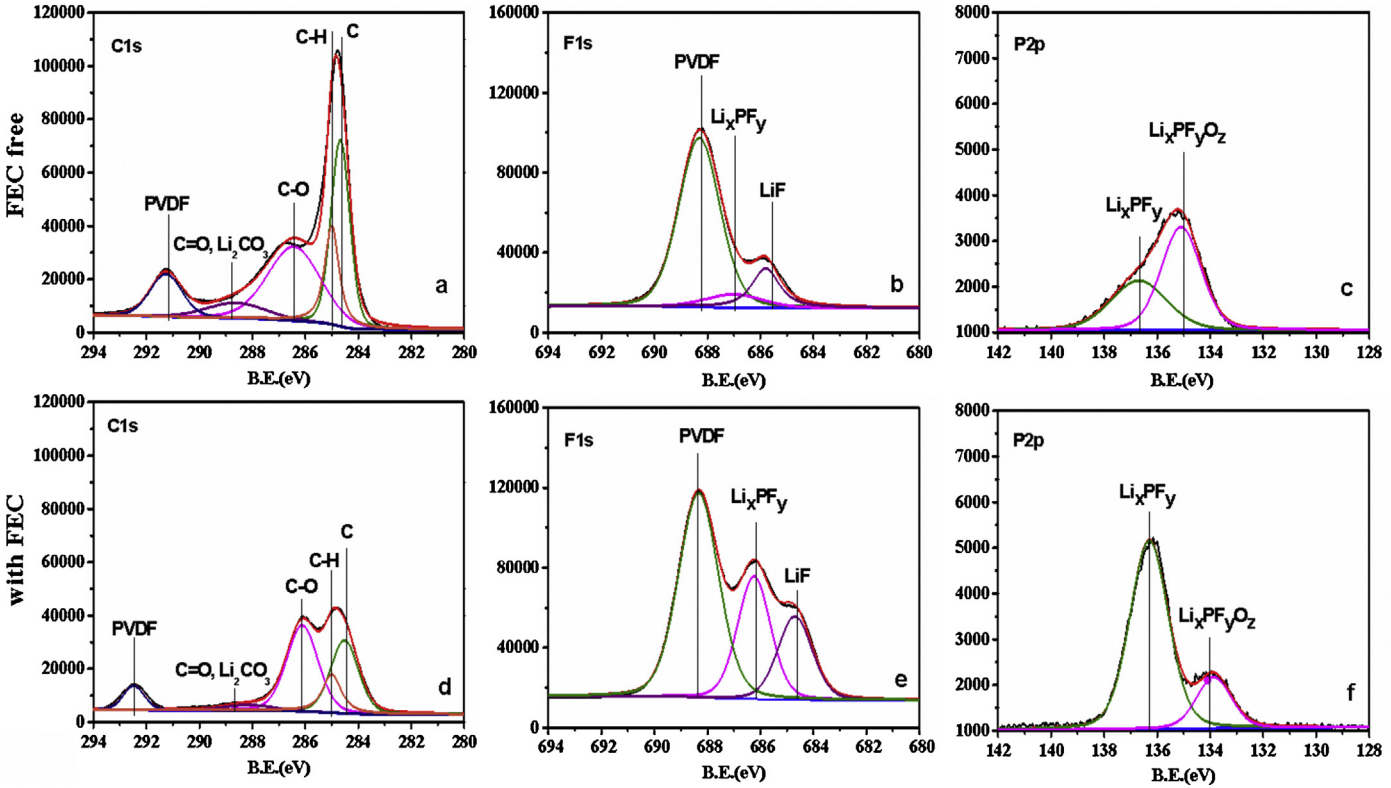

Fig. 8. C1s, F1s and P2p XPS spectra of the cycled $Li_{1.16}[Mn_{0.75}Ni_{0.25}]_{0.84}O_2$ electrodes in electrolytes without (a, b, c) and with 1% FEC (d, e, f) at 0.5C after 100 cycles.

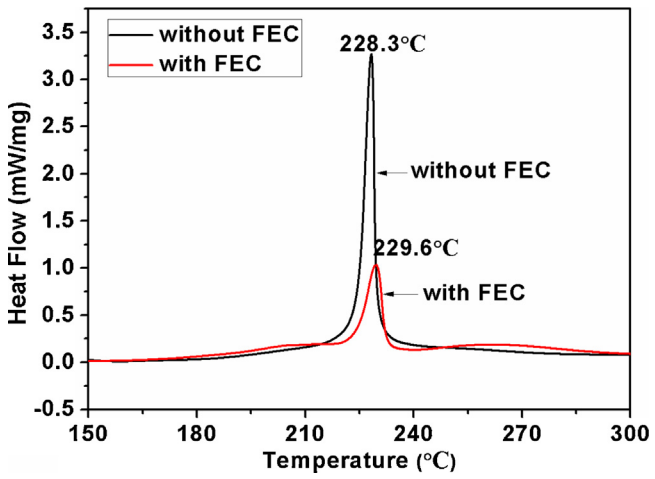

Fig. 9. DSC curves of fully delithiated $Li_{1.16}[Mn_{0.75}Ni_{0.25}]_{0.84}O_2$ cathode (charged to 4.7 V) without and with 1% FEC additive.

$$LiPF_6 \rightarrow LiF + PF_5 \quad (4)$$

$$PF_6^- - e^- \rightarrow PF_6^{\bullet} \rightarrow PF_5 + F^{\bullet} \rightarrow HF \quad (5)$$

$$PF_5 + 2ne^- + 2nLi^+ \rightarrow nLiF + mLi_xPF_y \quad (6)$$

$$LiPF_6 + H_2O \rightarrow LiF + OPF_3 + 2HF \quad (7)$$

$$PF_5 + H_2O \rightarrow OPF_3 + 2HF \quad (8)$$

$$OPF_3 + nH_2O + xLi^+ \rightarrow Li_xPO_yF_z + 2nHF \quad (9)$$

$$mOPF_3 + ne^- + nLi^+ \rightarrow LiF + mLi_xPO_yF_z \quad (10)$$

3.8. Differential scanning calorimetry (DSC)

To investigate the effect of FEC on the thermal stability of lithium rich cathode, a comparative study was conducted on fully charged cells with and without FEC. Fig. 9 exhibits the DSC heat flow curves at a scan rate of 5 °C/min for fully delithiated $Li_{1.16}[Mn_{0.75}Ni_{0.25}]_{0.84}O_2$ cells with and without FEC, respectively. The FEC-absence sample shows an exothermic peak at 228.3 °C with a heat flow of 3267.3 mW/g, while the peak temperature shifts to higher temperature (229.6 °C) and the released heat decreases to 1032.0 mW/g for FEC-containing one. The heat generated from the thermal decomposition reaction between the delithiated cathode and the electrolyte, is reduced by nearly 70% in presence of FEC. It implies that FEC enhances the thermal stability of the lithium rich cathode material [17,53]. In the case, FEC acts as a film-formation additive to build a more stable interphase between $Li_{1.16}[Mn_{0.75}Ni_{0.25}]_{0.84}O_2$ cathode and electrolyte, which protects the highly oxidative cathode particles from direct contact with the electrolyte solution and reduces the exothermic reaction. Therefore, the thermal stability of the charged $Li_{1.16}[Mn_{0.75}Ni_{0.25}]_{0.84}O_2$ cathode has been enhanced by introduction of FEC additive.

5. Conclusion

FEC as the electrolyte additive exhibits effects on the improved electrochemical performances of lithium rich cathode $Li_{1.16}[Mn_{0.75}Ni_{0.25}]_{0.84}O_2$. Advanced oxidative stability of the electrolyte has been obtained with FEC additive, moreover the larger binding energy value of FEC-PF_6^- complex implies the preferential reaction of FEC on cathode during charging. The studies demonstrate that a stable conductive SEI layer on the cathode has been formed in the cells with 1% and 2% FEC, which stabilizes the electrode/electrolyte interface and effectively suppresses the side reaction between electrode and electrolyte. It is concluded that FEC improves the compatibility between lithium-rich cathode and electrolyte via in situ forming the stabilized interfacial film.

Acknowledgements

This work was financially supported by the National 863 Program of China (No. 2013AA050901).

References

[1] M.M. Thackeray, C. Wolverton, E.D. Isaacs, Electrical energy storage for transportation–approaching the limits of, and going beyond, lithium-ion batteries, Energy Environ. Sci. 5 (2012) 7854–7863.
[2] Z. Lu, D.D. MacNeil, J.R. Dahn, Layered Cathode Materials $Li[Ni_xLi_{(1/3-2x/3)}Mn_{(2/3-x/3)}]O_2$ for Lithium-Ion Batteries, Electrochem. Solid-State Lett. 4 (2001) A191–A194.
[3] K. Kang, Y.S. Meng, J. Breger, C.P. Grey, G. Ceder, Electrodes with high power and high capacity for rechargeable lithium batteries, Science 311 (2006) 977–980.
[4] A.R. Armstrong, M. Holzapfel, P. Novák, C.S. Johnson, S.-H. Kang, M.M. Thackeray, P.G. Bruce, Demonstrating Oxygen Loss and Associated Structural Reorganization in the Lithium Battery Cathode $Li[Ni_{0.2}Li_{0.2}Mn_{0.6}]O_2$, J. Am. Chem. Soc. 128 (2006) 8694–8698.
[5] H. Yu, H. Zhou, High-Energy Cathode Materials (Li_2MnO_3–$LiMO_2$) for Lithium-Ion Batteries, J. Phys. Chem. Lett. 4 (2013) 1268–1280.
[6] M. Gu, A. Genc, I. Belharouak, D. Wang, K. Amine, S. Thevuthasan, D.R. Baer, J.-G. Zhang, N.D. Browning, J. Liu, C. Wang, Nanoscale Phase Separation, Cation Ordering, and Surface Chemistry in Pristine $Li_{1.2}Ni_{0.2}Mn_{0.6}O_2$ for Li-Ion Batteries, Chem. Mater. 25 (2013) 2319–2326.
[7] M.M. Thackeray, S.-H. Kang, C.S. Johnson, J.T. Vaughey, R. Benedek, S.A. Hackney, Li_2MnO_3-stabilized $LiMO_2$ (M = Mn, Ni Co) electrodes for lithium-ion batteries, J. Mater. Chem. 17 (2007) 3112–3125.
[8] M. Gao, F. Lian, H. Liu, C. Tian, L. Ma, W. Yang, Synthesis and electrochemical performance of long lifespan Li-rich $Li_{1+x}(Ni_{0.37}Mn_{0.63})_{1-x}O_2$ cathode materials for lithium-ion batteries, Electrochim. Acta 95 (2013) 87–94.
[9] F. Wu, N. Li, Y. Su, H. Lu, L. Zhang, R. An, Z. Wang, L. Bao, S. Chen, Can surface modification be more effective to enhance the electrochemical performance of lithium rich materials, J. Mater. Chem. 22 (2012) 1489–1497.
[10] J. Zheng, M. Gu, A. Genc, J. Xiao, P. Xu, X. Chen, Z. Zhu, W. Zhao, L. Pullan, C. Wang, J.G. Zhang, Mitigating voltage fade in cathode materials by improving the atomic level uniformity of elemental distribution, Nano Lett. 14 (2014) 2628–2635.
[11] Y.K. Sun, M.J. Lee, C.S. Yoon, J. Hassoun, K. Amine, B. Scrosati, The role of AlF_3 coatings in improving electrochemical cycling of Li-enriched nickel-manganese oxide electrodes for Li-ion batteries, Adv. Mater. 24 (2012) 1192–1196.
[12] J. Zheng, M. Gu, J. Xiao, B.J. Polzin, P. Yan, X. Chen, C. Wang, J. Zhang, Functioning mechanism of AlF_3 coating on the Li- and Mn-Rich cathode materials, Chem. Mater. 26 (2014) 6320–6327.
[13] G. Singh, R. Thomas, A. Kumar, R.S. Katiyar, A. Manivannan, Electrochemical and Structural Investigations on ZnO Treated 0.5 Li_2MnO_3-0.5$LiMn_{0.5}Ni_{0.5}O_2$ Layered Composite Cathode Material for Lithium Ion Battery, J. Electrochem. Soc. 159 (2012) A470–A478.
[14] Z. Wang, E. Liu, C. He, C. Shi, J. Li, N. Zhao, Effect of amorphous $FePO_4$ coating on structure and electrochemical performance of $Li_{1.2}Ni_{0.13}Co_{0.13}Mn_{0.54}O_2$ as cathode material for Li-ion batteries, J. Power Sources 236 (2013) 25–32.
[15] K. Xu, Electrolytes and interphases in Li-ion batteries and beyond, Chem. Rev. 114 (2014) 11503–11618.
[16] S.S. Zhang, A review on electrolyte additives for lithium-ion batteries, J. Power Sources 162 (2006) 1379–1394.
[17] Z.D. Li, Y.C. Zhang, H.F. Xiang, X.H. Ma, Q.F. Yuan, Q.S. Wang, C.H. Chen, Trimethyl phosphite as an electrolyte additive for high-voltage lithium-ion batteries using lithium-rich layered oxide cathode, J. Power Sources 240 (2013) 471–475.
[18] Y.-S. Kang, T. Yoon, S.S. Lee, J. Mun, M.S. Park, J.-H. Park, S.-G. Doo, I.-Y. Song, S. M. Oh, 1,3,5-Trihydroxybenzene as a film-forming additive for high-voltage positive electrode, Electrochem. Commun. 27 (2013) 26–28.

[19] J. Zhang, J. Wang, J. Yang, Y. NuLi, Artificial Interface Deriving from Sacrificial Tris(trimethylsilyl) phosphate Additive for Lithium Rich Cathode Materials, Electrochim. Acta 117 (2014) 99–104.
[20] S. Tan, Z. Zhang, Y. Li, J. Zheng, Z. Zhou, Y. Yang, Tris(hexafluoro-iso-propyl) phosphate as an SEI-Forming Additive on Improving the Electrochemical Performance of the $Li[Li_{0.2}Mn_{0.56}Ni_{0.16}Co_{0.08}]O_2$ Cathode Material, J. Electrochem. Soc. 160 (2013) A285–A292.
[21] M. Hu, J. Wei, L. Xing, Z. Zhou, Effect of lithium difluoro(oxalate) borate (LiDFOB) additive on the performance of high-voltage lithium-ion batteries, J. Appl. Electrochem. 42 (2012) 291–296.
[22] Y. Zhu, Y. Li, M. Bettge, D.P. Abraham, Positive Electrode Passivation by LiDFOB Electrolyte Additive in High-Capacity Lithium-Ion Cells, J. Electrochem. Soc. 159 (2012) A2109–A2117.
[23] S.J. Lee, J.G. Han, I. Park, J. Song, J. Cho, J.S. Kim, N.S. Choi, Effect of Lithium Bis (oxalato) borate Additive on Electrochemical Performance of $Li_{1.17}Ni_{0.17}Mn_{0.5}Co_{0.17}O_2$ Cathodes for Lithium-Ion Batteries, J. Electrochem. Soc. 161 (2014) A2012–A2019.
[24] R. Elazari, G. Salitra, G. Gershinsky, A. Garsuch, A. Panchenko, D. Aurbach, Rechargeable lithiated silicon–sulfur (SLS) battery prototypes, Electrochem. Commun. 14 (2012) 21–24.
[25] H. Nakai, T. Kubota, A. Kita, A. Kawashima, Investigation of the Solid Electrolyte Interphase Formed by Fluoroethylene Carbonate on Si Electrodes, J. Electrochem. Soc. 158 (2011) A798–A801.
[26] N.N. Sinha, J.C. Burns, J.R. Dahn, Storage Studies on Li/Graphite Cells and the Impact of So-Called SEI-Forming Electrolyte Additives, J. Electrochem. Soc. 160 (2013) A709–A714.
[27] S.-K. Jeong, M. Inaba, R. Mogi, Y. Iriyama, T. Abe, Z. Ogumi, SEI-Surface Film Formation on a Graphite Negative Electrode in Lithium-Ion Batteries Atomic Force Microscopy Study on the Effects of Film-Forming Additives in Propylene Carbonate Solutions, Langmuir 17 (2001) 8281–8286.
[28] L. Liao, X. Cheng, Y. Ma, P. Zuo, W. Fang, G. Yin, Y. Gao, Fluoroethylene carbonate as electrolyte additive to improve low temperature performance of $LiFePO_4$ electrode, Electrochim. Acta 87 (2013) 466–472.
[29] B. Wu, Y. Ren, D. Mu, X. Liu, J. Zhao, F. Wu, Enhanced electrochemical performance of $LiFePO_4$ cathode with the addition of fluoroethylene carbonate in electrolyte, J. Solid State Electrochem. 17 (2012) 811–816.
[30] Y. Park, S.H. Shin, H. Hwang, S.M. Lee, S.P. Kim, H.C. Choi, Y.M. Jung, Investigation of solid electrolyte interface (SEI) film on $LiCoO_2$ cathode in fluoroethylene carbonate (FEC)-containing electrolyte by 2D correlation X-ray photoelectron spectroscopy (XPS), J. Mol. Struct. 1069 (2014) 157–163.
[31] E. Markevich, G. Salitra, K. Fridman, R. Sharabi, G. Gershinsky, A. Garsuch, G. Semrau, M.A. Schmidt, D. Aurbach, Fluoroethylene carbonate as an important component in electrolyte solutions for high-voltage lithium batteries: role of surface chemistry on the cathode, Langmuir 30 (2014) 7414–7424.
[32] R. Sharabi, E. Markevich, K. Fridman, G. Gershinsky, G. Salitra, D. Aurbach, G. Semrau, M.A. Schmidt, N. Schall, C. Bruenig, Electrolyte solution for the improved cycling performance of $LiCoPO_4$/C composite cathodes, Electrochem. Commun. 28 (2013) 20–23.
[33] L. Yu, W. Qiu, F. Lian, J. Huang, X. Kang, Understanding the phenomenon of increasing capacity of layered $0.65Li[Li_{1/3}Mn_{2/3}]O_2 \cdot 0.35Li(Ni_{1/3}Co_{1/3}Mn_{1/3})O_2$, Journal of Alloys and Compounds 471 (2009) 317–321.
[34] H.-B. Han, K. Liu, S.-W. Feng, S.-S. Zhou, W.-F. Feng, J. Nie, H. Li, X.-J. Huang, H. Matsumoto, M. Armand, Z.-B. Zhou, Ionic liquid electrolytes based on multi-methoxyethyl substituted ammoniums and perfluorinated sulfonimides: Preparation, characterization, and properties, Electrochim. Acta 55 (2010) 7134–7144.
[35] S. Zugmann, M. Fleischmann, M. Amereller, R.M. Gschwind, H.D. Wiemhöfer, H.J. Gores, Measurement of transference numbers for lithium ion electrolytes via four different methods, a comparative study, Electrochim. Acta 56 (2011) 3926–3933.
[36] Aadil Benmayza, Wenquan Lu, Vijay Ramani, J. Prakash, Electrochemical and Thermal Studies of $LiNi_{0.8}Co_{0.15}Al_{0.015}O_2$ under Fluorinated Electrolytes, Electrochim. Acta 123 (2014) 7–13.
[37] R.L. Wang, C. Buhrmester, J.R. Dahn, Calculations of Oxidation Potentials of Redox Shuttle Additives for Li-Ion Cells, J. Electrochem. Soc. 153 (2006) A445–A449.
[38] E.G. Leggesse, J.-C. Jiang, Theoretical Study of the Reductive Decomposition of Ethylene Sulfite A Film-Forming Electrolyte Additive in Lithium Ion Batteries, J. Phys. Chem. A 116 (2012) 11025–11033.
[39] O. Borodin, T.R. Jow, Quantum Chemistry Studies of the Oxidative Stability of Carbonate, Sulfone and Sulfonate-Based Electrolytes Doped with BF_4^- PF_6^- Anions, ECS Trans. 33 (2011) 77–84.
[40] L. Xing, O. Borodin, G.D. Smith, W. Li, Density Functional Theory Study of the Role of Anions on the Oxidative Decomposition Reaction of Propylene Carbonate, J. Phys. Chem. A 115 (2011) 13896–13905.
[41] W.-J. Zhang, A review of the electrochemical performance of alloy anodes for lithium-ion batteries, J. Power Sources 196 (2011) 13–24.
[42] S.K. Martha, J. Nanda, G.M. Veith, N.J. Dudney, Surface studies of high voltage lithium rich composition: $Li_{1.2}Mn_{0.525}Ni_{0.175}Co_{0.1}O_2$, J. Power Sources 216 (2012) 179–186.
[43] L. Yang, T. Markmaitree, B.L. Lucht, Inorganic additives for passivation of high voltage cathode materials, J. Power Sources 196 (2011) 2251–2254.
[44] N. Yabuuchi, K. Yoshii, S.T. Myung, I. Nakai, S. Komaba, Detailed studies of a high-capacity electrode material for rechargeable batteries, Li_2MnO_3-$LiCo_{(1/3)}Ni_{(1/3)}Mn_{(1/3)}O_2$, Journal of the American Chemical Society 133 (2011) 4404–4419.
[45] J. Hong, H.-D. Lim, M. Lee, S.-W. Kim, H. Kim, S.-T. Oh, G.-C. Chung, K. Kang, Critical Role of Oxygen Evolved from Layered Li–Excess Metal Oxides in Lithium Rechargeable Batteries, Chemistry of Materials 24 (2012) 2692–2697.
[46] I.A. Profatilova, S.-S. Kim, N.-S. Choi, Enhanced thermal properties of the solid electrolyte interphase formed on graphite in an electrolyte with fluoroethylene carbonate, Electrochim. Acta 54 (2009) 4445–4450.
[47] K. Xu, Nonaqueous Liquid Electrolytes for Lithium-Based Rechargeable Batteries, Chem. Rev. 104 (2004) 4303–4417.
[48] R. Mogi, M. Inaba, Y. Iriyama, T. Abe, Z. Ogumi, Study of the Decomposition of Propylene Carbonate on Lithium Metal Surface by Pyrolysis-Gas Chromatography-Mass Spectroscopy, Langmuir 19 (2003) 814–821.
[49] V. Etacheri, O. Haik, Y. Goffer, G.A. Roberts, I.C. Stefan, R. Fasching, D. Aurbach, Effect of fluoroethylene carbonate (FEC) on the performance and surface chemistry of Si-nanowire Li-ion battery anodes, Langmuir 28 (2012) 965–976.
[50] Y. Okamoto, Decomposition Mechanism of Ethylene Carbonate and Fluoroethylene Carbonate through Hydrogen Abstraction under High Voltage Environment: An Ab-Initio Study, J. Electrochem. Soc. 161 (2014) A1527–A1533.
[51] S. Malmgren, K. Ciosek, M. Hahlin, T. Gustafsson, M. Gorgoi, H. Rensmo, K. Edström, Comparing anode and cathode electrode/electrolyte interface composition and morphology using soft and hard X-ray photoelectron spectroscopy, Electrochim. Acta 97 (2013) 23–32.
[52] A.J. Gmitter, I. Plitz, G.G. Amatucci, High Concentration Dinitrile, 3-Alkoxypropionitrile, and Linear Carbonate Electrolytes Enabled by Vinylene and Monofluoroethylene Carbonate Additives, J. Electrochem. Soc. 159 (2012) A370–A379.
[53] H.F. Xiang, H. Wang, C.H. Chen, X.W. Ge, S. Guo, J.H. Sun, W.Q. Hu, Thermal stability of $LiPF_6$-based electrolyte and effect of contact with various delithiated cathodes of Li-ion batteries, J. Power Sources 191 (2009) 575–581.